applied optics

Hybrid optical turbulence models using machine-learning and local measurements

Christopher Jellen,[1,*] Charles Nelson,[2] John Burkhardt,[1] and Cody Brownell[1]

[1]Mechanical Engineering Department, United States Naval Academy, 590 Holloway Rd., Annapolis, Maryland 21402, USA
[2]Electrical and Computer Engineering Department, United States Naval Academy, 597 McNair Rd., Annapolis, Maryland 21402, USA
*cdjellen@gmail.com

Received 13 February 2023; revised 19 May 2023; accepted 19 May 2023; posted 22 May 2023; published 13 June 2023

Accurate prediction of atmospheric optical turbulence in localized environments is essential for estimating the performance of free-space optical systems. Macro-meteorological models developed to predict turbulent effects in one environment may fail when applied in new environments. However, existing macro-meteorological models are expected to offer some predictive power. Building a new model from locally measured macro-meteorology and scintillometer readings can require significant time and resources, as well as a large number of observations. These challenges motivate the development of a machine-learning informed hybrid model framework. By combining a baseline macro-meteorological model with local observations, hybrid models were trained to improve upon the predictive power of each baseline model. Comparisons between the performance of the hybrid models, selected baseline macro-meteorological models, and machine-learning models trained only on local observations, highlight potential use cases for the hybrid model framework when local data are expensive to collect. Both the hybrid and data-only models were trained using the gradient boosted decision tree architecture with a variable number of *in situ* meteorological observations. The hybrid and data-only models were found to outperform three baseline macro-meteorological models, even for low numbers of observations, in some cases as little as one day. For the first baseline macro-meteorological model investigated, the hybrid model achieves an estimated 29% reduction in the mean absolute error using only one day-equivalent of observation, growing to 41% after only two days, and 68% after 180 days-equivalent training data. The data-only model generally showed similar, but slightly lower performance, as compared to the hybrid model. Notably, the hybrid model's performance advantage over the data-only model dropped below 2% near the 24 days-equivalent observation mark and trended towards 0% thereafter. The number of days-equivalent training data required by both the hybrid model and the data-only model is potentially indicative of the seasonal variation in the local microclimate and its propagation environment.

https://doi.org/10.1364/AO.487280

1. INTRODUCTION

Atmospheric optical turbulence degrades the performance of free-space optics (FSO) and other optical systems, especially at low altitudes and in the near-maritime environment [1–4]. These effects are characterized by the refractive index structure parameter, C_n^2. For horizontal propagation, under the assumption of isotropy and path-wise homogeneity, fluctuations in C_n^2 are dominated by temperature fluctuations [1]. The impact of atmospheric factors on C_n^2 led to the development of models which predict local turbulent effects from macro-meteorological features [2,5–7].

Existing macro-meteorological models are often extended to new microclimates in an attempt to generate optical turbulence predictions using local atmospheric feature measurements. These models may generate predictions with a higher error when applied to these new microclimates than in the environment in which the model was originally developed [2,8–10]. Some state-of-the-art models have performed well across similar microclimates, including the Navy Atmospheric Vertical Surface Layer Model (NAVSLaM), which performed well for both coastal and near-maritime propagation paths [11]. However, the equipment required to effectively measure potential temperature and wind shear gradients for state-of-the-art model predictions is often unavailable or cost prohibitive [2]. Additionally, developing a new model for each microclimate requires significant time, equipment, and expertise. Existing models may hold some predictive power across a range of propagation environments and may have the potential for augmentation, rather than full redevelopment.

These challenges motivate investigation into the development of the hybrid model framework. The hybrid model couples existing macro-meteorological models developed for similar microclimates along with some minimal amount of locally acquired meteorological and C_n^2 data. The hybrid model framework consists of two components, a baseline

macro-meteorological model and a machine-learning model trained on that baseline macro-meteorological model's residual error over the locally acquired training measurements. Under this approach, the hybrid model's predictions are the baseline macro-meteorological model's predictions augmented by a correction learned from locally measured meteorological and C_n^2 data. In this paper, the hybrid model approach is investigated with great detail for one specific baseline macro-meteorological model, as well as for a single propagation path; however, the hybrid model approach itself is not presented in this paper as being specific to any one model, architecture, or microclimate. To that end, two additional baseline models are evaluated to demonstrate the extensibility and potential limitations of the hybrid model approach.

Using locally acquired scintillometer and weather station measurements collected over the Severn River for approximately 31 months, a hybrid model was developed and compared against both a data-only model trained under the gradient boosted decision tree (GBDT) architecture in [12] using local measurements, and one specific baseline macro-meteorological model developed for a similar microclimate and presented in [7]. This particular macro-meteorological model was chosen as a baseline model because of its emphasis on the air–water temperature difference along the propagation path, similar to [8]. Both the hybrid and data-only models were trained with a variable number of bootstrapped training observations to investigate the marginal improvement in prediction accuracy resulting from more training observations.

The hybrid model framework demonstrated a significant improvement in predictive performance when compared to the baseline macro-meteorological models in [2,5,7], even with a very limited number of training observations. For example, in comparison with the baseline model presented in [7], and with only one day-equivalent data observation, the hybrid model demonstrated an estimated 29% improvement in the mean absolute error (MAE) in predicting $\mathrm{Log}_{10} C_n^2$. Additionally, the hybrid model's performance improved steadily, with an estimated 68% improvement using 180 days-equivalent of observation, and then saw marginal improvement thereafter.

2. METHOD

The principle aim of this study was to develop and analyze the hybrid model framework, which combines a baseline macro-meteorological model for predicting C_n^2 from local measurements with a machine-learning model trained to predict the baseline model's residual error in the local microclimate. For this study, the GBDT architecture was selected to learn the baseline model's residual error, and the hybrid model was compared to a data-only model of similar architecture trained using only local measurements.

The GBDT component of the hybrid model was trained on training observations of meteorological parameters and a target correction, tc, tailored to the baseline model's predicted $\mathrm{Log}_{10} C_n^2$, as expressed in Eq. (1):

$$\mathrm{tc} = \mathrm{Log}_{10} C_{n\,\mathrm{observed}}^2 - \mathrm{Log}_{10} C_{n\,\mathrm{baseline\ model\ predicted}}^2. \quad (1)$$

After training, the GBDT component of the hybrid model was used to predict a correction, $\hat{\mathrm{tc}}$, from new meteorological parameter observations. The predicted $\mathrm{Log}_{10}\, C_n^2$ of the baseline model is then adjusted by the hybrid model GBDT component's predicted tc for an observed vector of meteorological parameter using Eq. (2):

$$\mathrm{hybrid}\ \mathrm{Log}_{10} C_n^2 = \mathrm{Log}_{10} C_{n\,\mathrm{baseline\ model\ predicted}}^2 + \hat{\mathrm{tc}}. \quad (2)$$

The predicted $\mathrm{Log}_{10} C_n^2$ generated by the hybrid model is thus a composite of the baseline macro-meteorological model's prediction and the GBDT component's predicted tc. This prediction is the hybrid model's output, given an observed vector of macro-meteorological measurements. The hybrid model's GBDT component seeks to learn the mapping between local meteorological data and the baseline model's residuals, such that the composite prediction demonstrates a lower error than the baseline model alone.

A secondary aim of this study was to determine the amount of locally acquired data required to train an effective hybrid model or a data-only model under the GBDT architecture. While the macro-meteorological parameters used to predict local C_n^2 are readily available, measured either by existing weather stations [13] or by commercial off-the-shelf hardware [14], the hybrid model framework requires some number of locally acquired C_n^2 measurements to learn appropriate local corrections. Determining the minimum number of required observation days to achieve some estimated improvement in performance, as well as the relationship between the long-term prediction error and number of training observations, will aid in operationalizing the hybrid model approach to new contexts and microclimates.

3. MEASUREMENT

A. Data Collection

To investigate optical turbulence in the low-altitude near-maritime environment, an 890 [m] propagation path was established over the Severn River in Annapolis, Maryland. A scintillometer was used to establish a measure of optical turbulence, C_n^2, with which to compare model predictions. The scintillometer link was approximately horizontal, with an elevation of 2 to 4 [m] over the surface of the water depending on tides. The average elevation of the link was estimated at 3 [m]. Significant land masses exist at either end of the propagation path; however, approximately 98% of the path is over water. This environment has been previously characterized as "near-maritime" and "littoral," distinct from open-ocean propagation environments and paths exclusively over land [3,4,8,9,15].

C_n^2 measurements and associated timestamps were captured across the BLS 450 scintillometer link pictured in Fig. 1. This link provided measures of optical turbulence for approximately 31 months and was used to develop the hybrid model and the data-only model, and to make comparisons with the selected baseline macro-meteorological model. A local weather station was deployed next to the receiver which captured macro-meteorological parameters such as air temperature, wind speed, pressure, humidity, and solar radiation [14]. Additionally, publicly available data from the nearest National Data Buoy Center (NDBC) data buoy were used to obtain hourly averaged water temperature readings for the local environment [13].

Fig. 1. Scintillometer propagation path with receiver (R) and transmitter (T) for the BLS 450 scintillometer across the Severn River in Annapolis, Maryland [16].

Table 1. Macro-Meteorological and Oceanographic Parameters Captured Near the Link (January 1, 2020, Through July 14, 2022)

Parameter	Data Source	Unit	Measurement Frequency	Number of Observations
C_n^2	BLS 450	$[m^{-\frac{2}{3}}]$	1 min	1,246,802
Water Temperature	NOAA Weather Station, NDBC Data Buoy	[°C]	1-hour	21,946
Air Temperature	Davis	[°C]	10 min	125,569
Atmospheric Pressure	Weather	[mBar]		126,510
Relative Humidity	Station	[%]		125,583
Solar Radiation		$[\frac{W}{m^2}]$		125,633
Wind Speed		$[\frac{m}{s}]$		126,512

More information about each of these data sources and their methodologies is available in [8,9,13]. The elevation of the local weather station was approximately 3 [m] above the mean lower low water line, with water temperature readings captured approximately 1 [m] below the mean lower low water line [13]. The measurements captured are described in Table 1.

Before evaluating macro-meteorological models and developing hybrid models for the local propagation environment, the macro-meteorological and oceanographic parameters in Table 1 were re-sampled and interpolated to provide 1 min estimates of each parameter of interest. Additionally, the temporal hour for each observation was calculated by subtracting the time captured by the BLS 450 scintillometer from that day's sunrise time, and the air–water temperature difference in °C was computed for each applicable observation.

4. MODEL TRAINING AND EVALUATION

A. Baseline Macro-Meteorological Model

The literature is rich with examples of regression-based models for predicting local optical turbulence effects from meteorological parameters [2,5–7]. These studies often seek to develop models based on macro-meteorology for their local propagation environment. Additionally, macro-meteorological models have shown some promise in generating predicted C_n^2 when applied to new propagation environments [2]. While these models tend to demonstrate impressive predictive power when employed in the environment in which they were developed, performance tends to degrade when models are applied in other propagation environments or over longer periods of time [2,15].

The near-maritime propagation environment at the United States Naval Academy has some seasonal variation in measured C_n^2, with a predicted dependence on the temperature difference between the air and water in the air-to-water boundary layer above the Severn River [4,8]. While this propagation path has an elevation near sea level, these characteristics are similar to other propagation environments over water, where seasonal variation in C_n^2 has been observed. The boundary-layer propagation path over Fuxian Lake, as measured at the Fuxian Solar Observatory, is one such environment [7]. Both locations have land masses at each end of the propagation path and are relatively flat in the immediate vicinity of the scintillometer link.

Macro-meteorological models were developed to predict boundary layer C_n^2 from local measurements at the Fuxian Solar Observatory [7]. The authors of [7] reference a model for predicting ground-level C_n^2 for "normal meteorological conditions" at Fuxian Solar Observatory as reproduced in Eq. (3) [7]:

$$C_n^2(0) = (2.05\Delta T^2 + 2.37\Delta T + 1.58) \times 10^{-16}. \quad \textbf{(3)}$$

Table 2. Descriptive Statistics for Measured and Predicted C_n^2 at a Height of 3 [m] (January 1, 2020, Through July 14, 2022)

	Air–Water Temperature Difference [°C]	Measured C_n^2 [$m^{-\frac{2}{3}}$]	Eq. (3) Predicted C_n^2 [$m^{-\frac{2}{3}}$]
Count	1,241,037	1,246,802	1,156,426
Mean	−0.4	1.845×10^{-14}	2.862×10^{-15}
Std.	4.34	3.646×10^{-14}	4.350×10^{-15}
Min.	−12.25	1.642×10^{-17}	6.200×10^{-17}
25%	−2.66	2.871×10^{-15}	3.087×10^{-16}
Median	−0.07	8.326×10^{-15}	1.193×10^{-15}
75%	3.11	2.091×10^{-14}	3.652×10^{-15}
Max	18.8	2.404×10^{-12}	5.339×10^{-14}

In Eq. (3), the predicted $C_n^2(0)$ is a function of only the measured air–water temperature difference ΔT. The value for $C_n^2(h)$ at a height h in [m] within the boundary layer can be calculated using Eq. (4) [7,17]:

$$C_n^2(h) = C_n^2(0) h^{-\frac{1}{3}} e^{\left(-\frac{h}{h_0}\right)}. \tag{4}$$

In Eq. (4), h_0 is a constant equal to 3200 [m], where h is a height within the local boundary layer. For the propagation path over the Severn River, h was taken as 3 [m].

First, in order to study and compare the applicability of Eq. (3) to this study's local propagation environment on the Severn River, predictions for $C_n^2(0)$ were scaled to a height of 3 [m] using Eq. (4). Then a comparison of the measured C_n^2 and the value of C_n^2 predicted for the same height using a combination of Eqs. (3) and (4) is presented in Table 2.

The predicted C_n^2 of the model presented in [7], captured in Table 2 as Eq. (3), is generally lower than the observed C_n^2 over the Severn River for the period between January 1, 2020, and July 14, 2022. This may be due to the altitude at which Eq. (3) was developed, approximately 1720 [m] above sea level [7], or the deleterious impact of local traffic and aerosols along the Severn River propagation path. Despite this general under-prediction, Eq. (3) provides a remarkably elegant tool for estimating local C_n^2 from measured air–water temperature difference alone. The prediction accuracy of Eq. (3) is further analyzed through the joint distribution of predicted and measured C_n^2 in Fig. 2.

Figure 2 highlights both the general under-prediction of C_n^2 in the propagation path over the Severn River, as well as the similar shape in the distributions between measured and predicted C_n^2. This under-prediction is most pronounced when the air–water temperature difference approaches 0 as identified in [4]. For the period between January 1, 2020, and July 14, 2022, the MAE in predicted $\mathrm{Log}_{10} C_n^2$ was 0.981, while the mean absolute percentage error (MAPE) was 7.02%. For the period between July 14, k, and July 14, 2022, the MAE in predicted $\mathrm{Log}_{10} C_n^2$ was 0.989, while the MAPE was 7.08%. These metrics establish a baseline for the level of accuracy with which an observer could predict C_n^2 from local macro-meteorological parameters using another model, in this case Eq. (3) which specifically utilized an air–water temperature difference, in the Severn River propagation environment. This study seeks to improve upon these predictions by developing a hybrid model, which couples both a macro-meteorological model, Eq. (3) with a GBDT model trained on its residuals as outlined in Eq. (1).

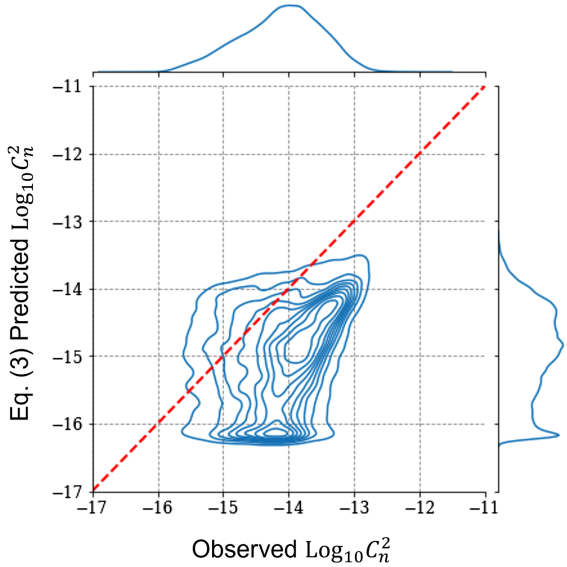

Fig. 2. Joint distribution of measured C_n^2 and the macro-meteorological model in Eq. (3)'s predicted C_n^2 at 3 [m] between January 1, 2020, and July 14, 2022.

B. Hybrid and Data-Only GBDT Models

Locally measured meteorological parameters and scintillometer readings of C_n^2 were used to train a hybrid and a data-only model under the GBDT architecture as described in [12]. Specifically, local C_n^2 data with a 1 min frequency, with some infrequent dropouts, were available between January 1, 2020, and July 14, 2022. The period between July 14, 2021, and July 14, 2022, contained 460,040 observations of C_n^2 alongside the meteorological parameters described in Table 1. These observations were set aside as a long-term validation set to evaluate the baseline model in Eq. (3), the hybrid model, and the data-only model. The remaining 696,386 observations of C_n^2 and local meteorological parameters were used to develop bootstrapped training samples. This serves both to estimate model performance with a given number of training observations, and to estimate the variability in validation set predictions for a model with a given number of training observations and architecture. 1440 of these 1 min observations, denoted as one "day-equivalent" of observation, were sampled randomly with replacement from the

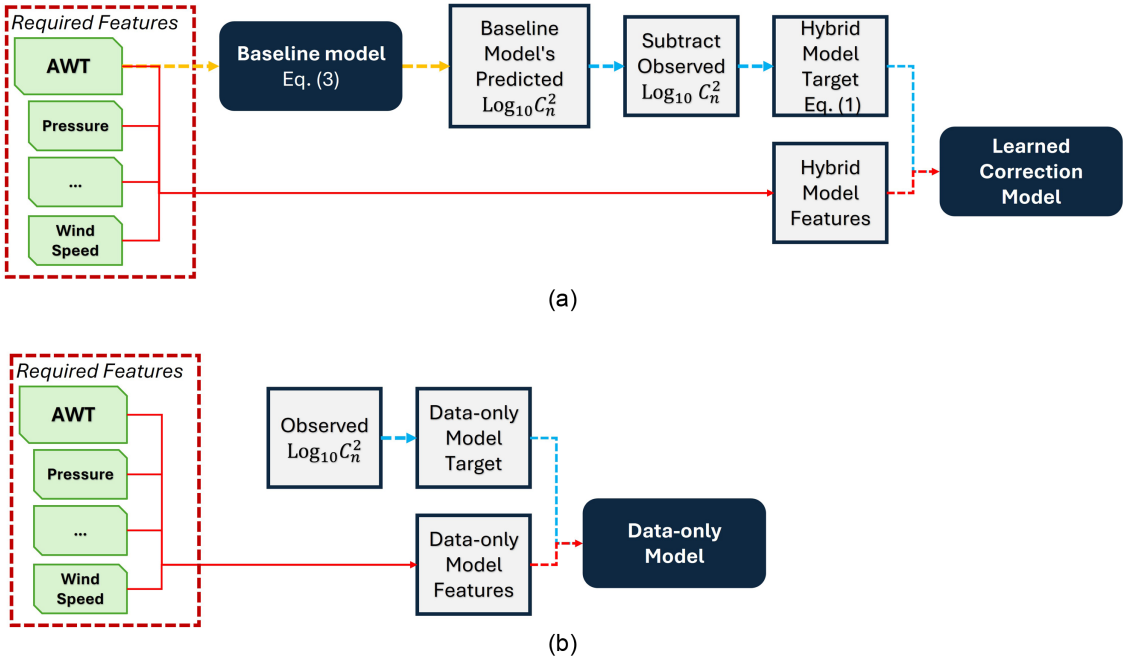

Fig. 3. Training processes for the (a) hybrid model and (b) data-only model.

Table 3. Possible Hyper-Parameter Combinations Used in Grid Search

Description	Hyper-Parameter Name [12,18]	Possible Values
Number of leaves for each constituent tree node.	`num_leaves`	8, 128, 512, 1024, 4096
Model learning rate under the gradient boosting framework.	`learning_rate`	0.5, 0.2, 0.1, 0.01
Minimum number of training observations in each leaf node of each constituent tree.	`min_data_in_leaf`	32, 128, 512, 2048, 4096

training set, which spanned from January 1, 2020, to July 14, 2021. Both the hybrid and data-only models leveraged the same meteorological parameters as training features. While the data-only model was trained to predict observed $\text{Log}_{10}C_n^2$ from those features alone, the hybrid model predicted $\text{Log}_{10}C_n^2$ following Eq. (2) from both these meteorological parameters and the baseline model in Eq. (3), as described in Fig. 3.

Both the hybrid and data-only models in Fig. 3 were trained to fit their target from their available features under the GBDT architecture. The GBDT architecture leverages model hyper-parameters in training to define the training and topology of constituent trees, and the way in which those trees are aggregated to form final model predictions [12,18]. An effort was made to identify reasonable hyper-parameters for a given number of days-equivalent observation using a grid search methodology [18]. The loss function was set to the MAE, with 512 trees used in each ensemble, and the GBDT methodology discussed in [12]. The possible hyper-parameters are described in Table 3.

Each possible combination of hyper-parameters in Table 3 was evaluated for every fifth number of days-equivalent observation in the training set, from 1 to 480, as described in Table 4. The combination of hyper-parameters in Table 3 with the lowest error in training a data-only model under the GBDT architecture was selected for both the data-only and hybrid models. Selecting reasonable hyper-parameters helps to improve each model's prediction accuracy for the given number of days-equivalent observation. The metrics, features, and target parameters are further described in Table 4.

In Table 4, both the hybrid and data-only models share the same set of features described in Table 1, along with the temporal hour and air–water temperature difference, interpolated to a 1 min frequency. The data-only model seeks to predict $\text{Log}_{10}C_n^2$ directly from these features, where the hybrid model seeks to predict the tc defined in Eq. (1), such that it can be combined with the log of the prediction generated by the baseline macro-meteorological model in Eq. (3) for a given observation vector to produce a hybrid $\text{Log}_{10}C_n^2$ following Eq. (2), as demonstrated in Fig. 4.

Both hybrid and data-only models in Fig. 4 were trained and evaluated using the features, hyper-parameters, and number of days-equivalent observation in Table 4. The hybrid and data-only models were evaluated for each number of days-equivalent observation across 20 iterations. Bootstrapped samples of the selected number of days-equivalent observation formed the training set in each iteration, and for each model. The hybrid and data-only models were evaluated under the MAE and MAPE metrics. The performance was averaged across the 20 iterations, which helped to estimate the mean and confidence interval for both the hybrid and data-only models for a given number of days-equivalent observation.

Table 4. Features and Hyper-Parameters Available in Hybrid and Data-only Model Training

Model	Target	Metric	Features	Number of Days-Equivalent Observations in Training Set	Hyper-Parameters
Data-Only	$\mathrm{Log}_{10} C_n^2$	MAE	Air–Water Temperature Difference, Wind Speed, Humidity, Pressure, Solar Radiation, Temporal Hour, Air–Water Temperature Difference	1	`learning_rate: 0.5`
				2	`min_data_in_leaf: 32`
				3	`num_leaves: 8`
				4	
				5	
Hybrid	Target correction (tc in Eq. (1))			6	`learning_rate: 0.1`
				7	`min_data_in_leaf: 128`
				8	`num_leaves: 8`
				9	
				10	
				12	`learning_rate: 0.1`
				14	`min_data_in_leaf: 128`
				16	`num_leaves: 8`
				18	
				21	
				24	`learning_rate: 0.1`
				27	`min_data_in_leaf: 128`
				30	`num_leaves: 8`
				45	
				60	
				75	`learning_rate: 0.01`
				90	`min_data_in_leaf: 128`
				120	`num_leaves: 8`
				150	
				180	
				210	`learning_rate: 0.01`
				240	`min_data_in_leaf: 512`
				270	`num_leaves: 128`
				300	
				330	
				360	`learning_rate: 0.01`
				390	`min_data_in_leaf: 128`
				420	`num_leaves: 1024`
				450	
				480	

5. RESULTS AND ANALYSIS

The bootstrapped mean and standard deviation of each metric in Table 4 was computed using the validation set, spanning one year from July 14, 2021, through July 14, 2022. By setting aside a one-year validation set, each model's performance across a range of seasonal conditions was evaluated. This validation set provides an estimate of long-term prediction accuracy for observations far removed from training data. These performance metrics are presented in Table 5 and visually in Fig. 5.

The Eq. (3) baseline model's predictions over the validation set were presented alongside Fig. 5, with the MAE in predicted $\mathrm{Log}_{10} C_n^2$ calculated as 0.989 and the MAPE was 7.08%. Based on the results in Table 5, the existing model can be improved using the hybrid model framework using only one day's worth of data, or a block of 1440 sequential 1 min observations. The MAE in predicted $\mathrm{Log}_{10} C_n^2$ trained on one day-equivalent observation for the hybrid model was estimated at 0.700, a 29% reduction compared against the existing model. Similarly, the data-only model's reduction in the error was estimated at 0.611, a 38% reduction compared against the existing model.

Both the hybrid and data-only models show similar gains in prediction accuracy when compared against the existing macro-meteorological model. These gains appear to level off somewhat after 180 sampled days-equivalent of observation. With 180 sampled days-equivalent of observation, the hybrid model had an estimated 68% reduction in the error, improving to a 69% reduction in the error with 480 sampled days-equivalent of observation. It is interesting to note that the hybrid model appears to minimally outperform the data-only model over much of the investigation period, but when the days-equivalent observation is less than 5, the data-only model marginally outperforms the hybrid model. From that point, the hybrid model is marginally more effective, with gains in performance falling below 2% near the 24 days-equivalent observation mark. The models trained with 1 to 180 days-equivalent are presented in greater detail in Fig. 6.

Figures 5 and 6 highlight three key results from this investigation. The first is that hybrid models, as well as a data-only

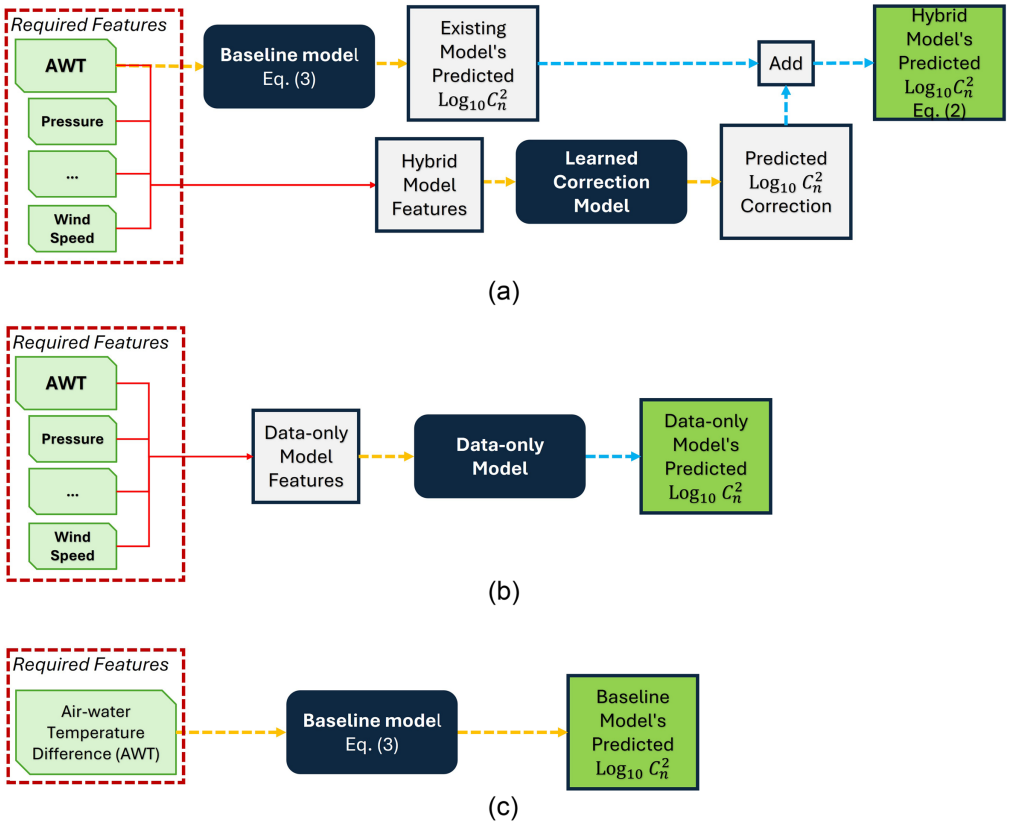

Fig. 4. Generating predicted $\text{Log}_{10}C_n^2$ from meteorological parameters using the (a) hybrid model, (b) data-only model, and (c) baseline model.

model, can significantly improve on a selected baseline model using as little as one day's observation from the local microclimate. The performance of the hybrid model was often within the confidence interval of the data-only model trained on the same number of bootstrapped samples. This convergence in performance is most evident in models trained with more than 18 days-equivalent of bootstrapped observations, as seen in Fig. 7.

In Fig. 7, the performance relative to Eq. (3) improves by approximately 58% under the data-only model and 59% under the hybrid model after 18 days-equivalent observation. Figures 5–7 highlight that both the data-only and hybrid models demonstrated improvements in prediction accuracy as more data was made available for training. However, the rate of improvement plateaus as more training observations are made available. This effect only appeared to slow substantially after at least 180 days-equivalent of bootstrapped samples were used in fitting the models.

Both the hybrid and data-only models are capable of leveraging *in situ* measurements of turbulent effects and meteorological parameters in generating improved predictions of C_n^2 when compared to the baseline model. With only one day-equivalent of observation, this performance improvement is estimated at approximately 29% in the MAE and MAPE of $\text{Log}_{10}C_n^2$. As more data are made available for training the data-only and hybrid models, this effect becomes more pronounced, with the prediction error falling by approximately 68% when 180 days-equivalent or more is available. To better understand the performance of the hybrid and data-only models, and their performance relative to the baseline model in Eq. (3), one of each model was trained using all available measurements in the training set. The hyper-parameters in the last row of Table 4 were selected for training. The improvement in prediction accuracy for validation set observations is captured in Fig. 8.

In Fig. 8, the hybrid model serves to adjust predictions for C_n^2 based on locally measured macro-meteorological parameters. When aggregated across the validation set, the hybrid model's prediction distribution in Fig. 8(b) more closely matches the observed distribution of $\text{Log}_{10}C_n^2$ than the initial prediction distribution in Fig. 8(a). While it does not fully capture the relationships between the local propagation environment and observed C_n^2, the hybrid model presents an improvement in aggregate prediction accuracy over the baseline in Eq. (3) when evaluated over the one-year validation set.

In addition to developing a hybrid model from the baseline model in Eq. (3), two additional literature models were augmented under the hybrid model framework to investigate the framework's extensibility. The macro-meteorological model presented in [5] was trained for an over-land propagation environment at a height of 15 [m], and captures diurnal variation in C_n^2. In order to generate predictions from local meteorological data, the dynamic range presented in [5] was applied, with measurements outside that dynamic range dropped from the training and validation sets. This model is presented in parametric form as

Table 5. Model Performance Against the Test Set for Hybrid and Data-Only Models Trained with Select Number of Days-Equivalent Observations

Number of Days-Equivalent Observations in Training Set	Mean Absolute % Error (validation set)				MAE $\mathrm{Log}_{10} C_n^2$ (validation set)			
	Hybrid Model		*Data-Only Model*		*Hybrid Model*		*Data-Only Model*	
	Bootstrap mean	*Bootstrap Std.*	*Bootstrap mean*	*Bootstrap Std.*	*Bootstrap mean*	*Bootstrap Std.*	*Bootstrap mean*	*Bootstrap Std.*
1	4.92%	0.78%	4.30%	0.74%	0.700	0.110	0.610	0.109
2	4.10%	0.70%	3.89%	0.43%	0.581	0.102	0.549	0.057
3	3.91%	0.54%	4.21%	0.58%	0.553	0.076	0.593	0.080
4	3.91%	0.50%	4.08%	0.52%	0.555	0.071	0.577	0.073
5	3.77%	0.71%	3.92%	0.61%	0.534	0.101	0.555	0.085
6	3.53%	0.52%	3.49%	0.39%	0.499	0.073	0.493	0.053
7	3.16%	0.44%	3.43%	0.50%	0.448	0.061	0.484	0.069
8	3.03%	0.14%	3.23%	0.25%	0.430	0.018	0.457	0.033
9	3.07%	0.23%	3.31%	0.24%	0.435	0.032	0.468	0.033
10	3.02%	0.24%	3.30%	0.27%	0.429	0.033	0.468	0.037
12	2.93%	0.19%	3.08%	0.28%	0.416	0.027	0.437	0.038
14	2.96%	0.30%	3.15%	0.29%	0.419	0.042	0.445	0.039
16	2.80%	0.18%	2.99%	0.25%	0.398	0.025	0.424	0.034
18	2.85%	0.16%	2.94%	0.24%	0.405	0.021	0.417	0.033
21	2.80%	0.20%	2.87%	0.20%	0.397	0.028	0.406	0.027
24	2.63%	0.11%	2.80%	0.12%	0.375	0.016	0.398	0.016
27	2.55%	0.14%	2.66%	0.14%	0.363	0.020	0.379	0.019
30	2.53%	0.09%	2.63%	0.11%	0.360	0.013	0.375	0.015
45	2.45%	0.08%	2.53%	0.09%	0.349	0.011	0.361	0.012
60	2.38%	0.05%	2.46%	0.06%	0.339	0.008	0.350	0.009
75	2.31%	0.05%	2.39%	0.07%	0.329	0.008	0.341	0.009
90	2.30%	0.05%	2.35%	0.05%	0.327	0.008	0.336	0.007
120	2.25%	0.03%	2.27%	0.04%	0.321	0.005	0.324	0.006
150	2.20%	0.04%	2.22%	0.05%	0.314	0.006	0.316	0.008
180	2.19%	0.03%	2.22%	0.03%	0.312	0.005	0.317	0.005
210	2.15%	0.03%	2.18%	0.03%	0.307	0.004	0.311	0.004
240	2.16%	0.03%	2.18%	0.04%	0.308	0.004	0.311	0.006
270	2.15%	0.03%	2.16%	0.04%	0.306	0.004	0.309	0.006
300	2.14%	0.03%	2.16%	0.04%	0.306	0.004	0.308	0.005
330	2.12%	0.03%	2.14%	0.03%	0.303	0.004	0.305	0.004
360	2.17%	0.02%	2.21%	0.03%	0.309	0.003	0.315	0.004
390	2.16%	0.02%	2.19%	0.02%	0.308	0.003	0.312	0.004
420	2.15%	0.01%	2.18%	0.03%	0.307	0.002	0.311	0.004
450	2.15%	0.02%	2.16%	0.02%	0.306	0.002	0.309	0.003
480	2.14%	0.02%	2.16%	0.02%	0.306	0.003	0.309	0.004

$$C_n^2 = (3.8 \times 10^{-14})W + f(T) + f(U) + f(\mathrm{RH}) - (5.3 \times 10^{-13}),$$

where

$$f(T) = (2.0 \times 10^{-15})T,$$

$$f(U) = (-2.5 \times 10^{-15})U + (1.2 \times 10^{-15})U^2 - (8.5 \times 10^{-15})U^3,$$

$$f(\mathrm{RH}) = (-2.8 \times 10^{-15})\mathrm{RH} + (2.9 \times 10^{-17})\mathrm{RH}^2 - (1.1 \times 10^{-19})\mathrm{RH}^3. \quad (5)$$

In Eq. (5), W denotes the temporal hour weight [5], T denotes the temperature in [K], RH denotes the relative humidity in [%], and U denotes the wind speed in $[\frac{\mathrm{m}}{\mathrm{S}}]$. Over the validation set between July 2021 and July 2022, Eq. (5) had a MAE in predicting $\mathrm{Log}_{10} C_n^2$ of 1.068. Using Eq. (5) as a baseline model, a hybrid model was developed to augment the predictions of Eq. (5) to the Severn River's microclimate. The scaling law in Eq. (4) was applied to generate predictions for a height of 3 [m]. With one day-equivalent observation, the MAE on the one-year validation set was reduced by 38%. After 7 days-equivalent observation, the improvement was 55%, growing to 69% after 180 days-equivalent observation. The effectiveness of the hybrid model approach in this context may be due to the greater disparity in the environment for which Eq. (5) was

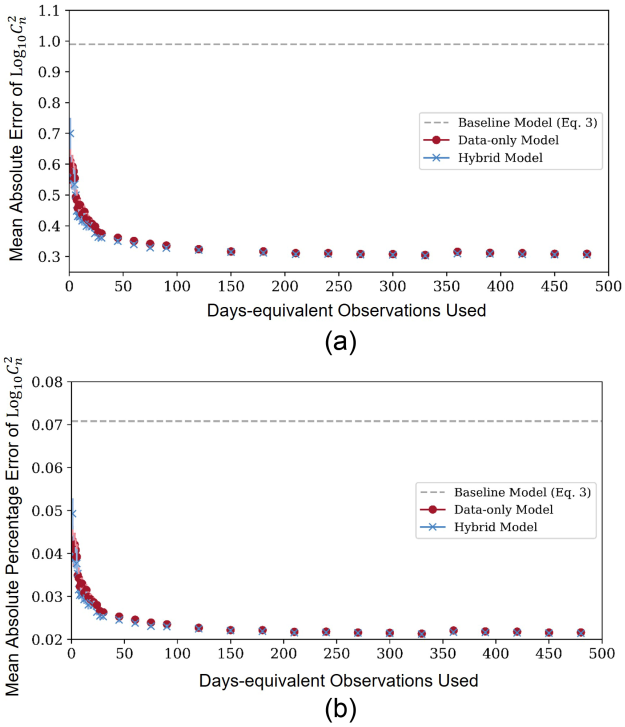

Fig. 5. (a) MAE and (b) MAPE with 95% confidence intervals for selected numbers of bootstrapped days-equivalent observations in model training.

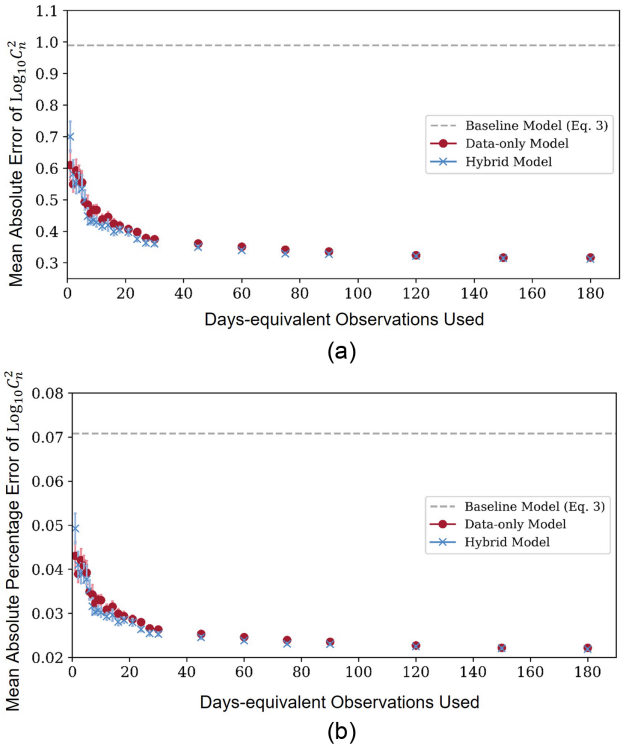

Fig. 6. (a) MAE and (b) MAPE with 95% confidence intervals for hybrid and data-only models trained with up to 180 bootstrap-sampled days-equivalent data.

developed, with a focus on over-land propagation rather than over-water, as in Eq. (3) [5,7].

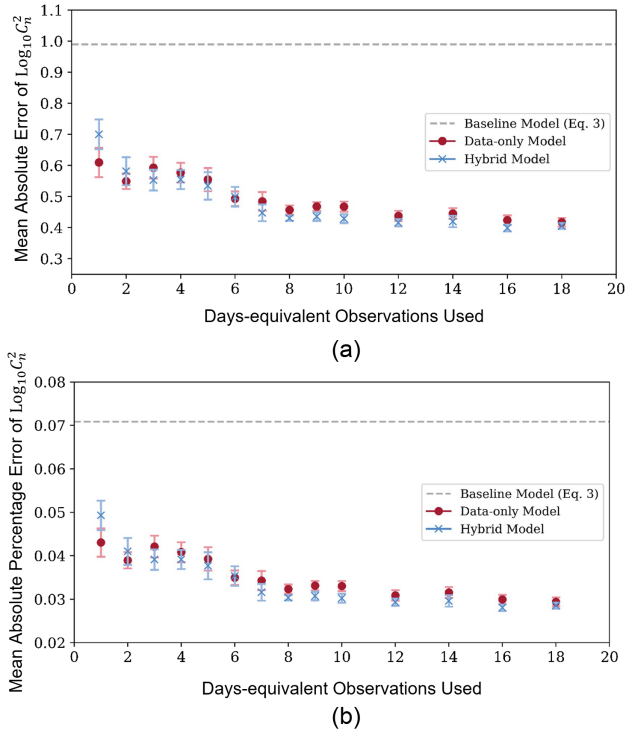

Fig. 7. (a) MAE and (b) MAPE with 95% confidence intervals for hybrid and data-only models trained with up to 18 days of bootstrap-sampled days-equivalent data.

The model described in Eq. (5) was analyzed and refit in [2] to better capture turbulent dynamics in a coastal environment. The "Offshore macrometeorological model of C_n^2" described in [2] is reproduced as

$$C_n^2 = (-1.58 \times 10^{-15})\,W + f(T) + f(U) + f(\mathrm{RH}) - (7.44 \times 10^{-14}),$$

where

$$f(T) = (2.74 \times 10^{-16})\,T,$$

$$f(U) = (3.37 \times 10^{-16})U + (1.92 \times 10^{-16})U^2 - (2.8 \times 10^{-17})U^3,$$

$$f(\mathrm{RH}) = (8.3 \times 10^{-17})\mathrm{RH} - (2.22 \times 10^{-18})\mathrm{RH}^2 + (1.42 \times 10^{-20})\mathrm{RH}^3. \quad \textbf{(6)}$$

In Eq. (6), W denotes the temporal hour weight [5], T denotes the temperature in [K], RH denotes the relative humidity in [%], and U denotes the wind speed in $[\frac{\mathrm{m}}{\mathrm{S}}]$. As for Eq. (5), measurements outside the dynamic range presented in [2] were removed from the training and validation sets. This model demonstrated a lower prediction error than that in Eq. (5) over the one-year validation set, with a MAE in predicted $\mathrm{Log}_{10}C_n^2$ of 0.533. Taking Eq. (6) as the baseline, the hybrid model approach failed to improve prediction accuracy in the one-day equivalent observation case, but improved the MAE by 8%

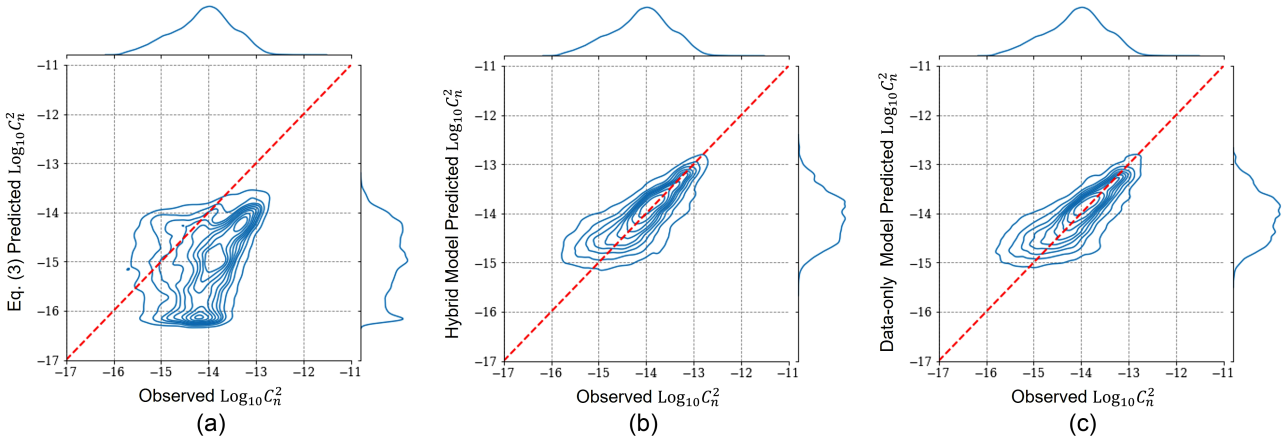

Fig. 8. Joint distribution of measured C_n^2 and the baseline model's predicted C_n^2 from Eq. (3) at 3 [m] on the validation set in (a) with hybrid model predictions in (b), and with a data-only model in (c).

at 7 days-equivalent observation and by 40% at 180 days-equivalent observation. The hybrid model approach with Eq. (6) as a baseline could indicate that, for baseline models well suited to the environments in which they are applied, more local measurements are required to improve prediction accuracy.

6. CONCLUSION

Macro-meteorological models which generate predicted C_n^2 from locally measured parameters present a useful baseline for efficiently estimating local turbulent effects. These macro-meteorological models often fail to capture the full extent of turbulent dynamics when applied in new propagation environments such as the air–water boundary layer above the Severn River. These challenges motivated the development of the hybrid model framework for augmenting baseline model predictions with corrections learned from a minimal amount of local observation. This hybrid model framework approach is investigated in detail with one selected baseline model, and then evaluated with two additional baseline macro-meteorological models over a single propagation path. The hybrid model framework approach itself is not specific to any baseline macro-meteorological model, architecture, or microclimate, and it may demonstrate similar performance improvements when extended to new baseline models, architectures, and domains. Both the hybrid model and the data-only model outperformed the baseline model, in some cases when only one day-equivalent of 1 min observation was available for training.

The hybrid model framework effectively augmented three baseline models, improving their prediction accuracy over a one-year validation set. For the Eq. (3) baseline, both the hybrid and data-only model's demonstrated similar performance and predictive power for a given number of bootstrapped samples, with the hybrid model marginally outperforming the data-only model after approximately the 5 days-equivalent observation mark. The hybrid models improved steadily through approximately 180 days-equivalent observation, and marginally thereafter. With only one day-equivalent of observation, the hybrid model's performance improvement is an estimated reduction in the MAE of approximately 29%, which grows to approximately 68% with 180 days-equivalent of observation. The absence of a total performance asymptote is potentially indicative of the seasonal variation in the local microclimate and its impact on C_n^2 over the propagation path.

While these models showed a remarkable increase in prediction accuracy when compared to the baseline models, architectures which better leverage temporal dependencies and the sequential nature of the data, or better handle missing values, may provide a source of further improvement. Further, as highlighted by the amount of data required to observe a possible asymptote in performance improvement, the seasonality of the local propagation environment merits further study. Its impact on the development of new models, especially when data are limited, may help explain the relationship between validation set prediction performance and the number of bootstrapped samples used in training the models.

Funding. Office of Academic Research, U.S. Naval Academy; Directed Energy Joint Technology Office; Office of Naval Resarch.

Acknowledgment. The authors would like to thank the meteorologists at the National Data Buoy Center for making their data available, and the team at the Water Front Readiness Center in Annapolis, MD, for their support in establishing the scintillometer link.

Disclosures. The authors declare no conflicts of interest.

Data availability. Data underlying the results presented in this paper are not publicly available at this time but may be obtained from the authors upon reasonable request.

REFERENCES

1. R. Barrios, F. Dios, and D. Narottam, "Wireless optical communications through the turbulent atmosphere: a review," in *Optical Communications Systems* (2012), pp. 1–40.
2. H. Wang, B. Li, X. Wu, C. Liu, Z. Hu, and P. Xu, "Prediction model of atmospheric refractive index structure parameter in coastal area," J. Mod. Opt. **62**, 1336–1346 (2015).
3. P. A. Frederickson, K. L. Davidson, C. R. Zeisse, and C. S. Bendall, "Estimating the refractive index structure parameter (C_n^2) over the ocean using bulk methods," J. Appl. Meteorol. **39**, 1770–1783 (2000).
4. P. A. Frederickson, S. Hammel, and D. Tsintikidis, "Measurements and modeling of optical turbulence in a maritime environment," Proc. SPIE **6303**, 630307 (2006).

5. D. Sadot and N. S. Kopeika, "Forecasting optical turbulence strength on the basis of macroscale meteorology and aerosols: models and validation," Opt. Eng. **31**, 200–212 (1992).
6. A. A. B. Raj, J. A. V. Selvi, and S. Durairaj, "Comparison of different models for ground-level atmospheric turbulence strength (C_n^2) prediction with a new model according to local weather data for FSO applications," Appl. Opt. **54**, 802–815 (2015).
7. L. Chen, Z. Liu, and D. Chen, "Climatological analysis of the seeing at Fuxian Solar observatory," Res. Astron. Astrophys. **19**, 015 (2019).
8. C. Jellen, J. Burkhardt, C. Brownell, and C. Nelson, "Machine learning informed predictor importance measures of environmental parameters in maritime optical turbulence," Appl. Opt. **59**, 6379–6389 (2020).
9. C. Jellen, C. Nelson, C. Brownell, J. Burkhardt, and M. Oakley, "Measurement and analysis of atmospheric optical turbulence in a near-maritime environment," IOP SciNotes **1**, 024006 (2020).
10. R. J. Oermann, "Novel methods for the quantification of atmospheric turbulence strength in the atmospheric surface layer," Ph.D. thesis (School of Chemistry and Physics, 2014).
11. R. Mahon, C. Moore, M. S. Ferraro, W. S. Rabinovich, and P. A. Frederickson, "Comparison of maritime measurements of C_n^2 with NAVSLaM model predictions," Appl. Opt. **59**, 10599–10612 (2020).
12. G. Ke, Q. Meng, T. Finley, T. Wang, W. Chen, W. Ma, Q. Ye, and T.-Y. Liu, "Lightgbm: A highly efficient gradient boosting decision tree," in *Advances in neural information processing systems* (2017), Vol. **30**.
13. National Data Buoy Center, "Station TPLM2 - Thomas Point, MD," 2022, https://www.ndbc.noaa.gov/station_history.php?station=tplm2.
14. Davis Instruments Corporation, "Vantage Pro2 Spec Sheets," 2023, https://support.davisinstruments.com/category/esfbscicgu-vantage-pro-2.
15. C. Jellen, C. Nelson, C. Brownell, J. Burkhardt, and M. Oakley, "Machine-learning informed macro-meteorological models for the near-maritime environment," Appl. Opt. **60**, 2938–2951 (2021).
16. Google Maps, "Aerial View of the United States Naval Academy," 2023, https://www.google.com/maps/@38.9824368,-76.4737818,957m/data=!3m1!1e3.
17. D. L. Fried, "Statistics of a geometric representation of wavefront distortion," J. Opt. Soc. Am. **55**, 1427–1435 (1965).
18. F. Pedregosa, G. Varoquaux, A. Gramfort, V. Michel, B. Thirion, O. Grisel, M. Blondel, P. Prettenhofer, R. Weiss, V. Dubourg, and J. Vanderplas, "Scikit-learn: machine learning in Python," J. Mach. Learn. Res **12**, 2825–2830 (2011).